RSC Advances

ROYAL SOCIETY OF CHEMISTRY

www.rsc.org/advances

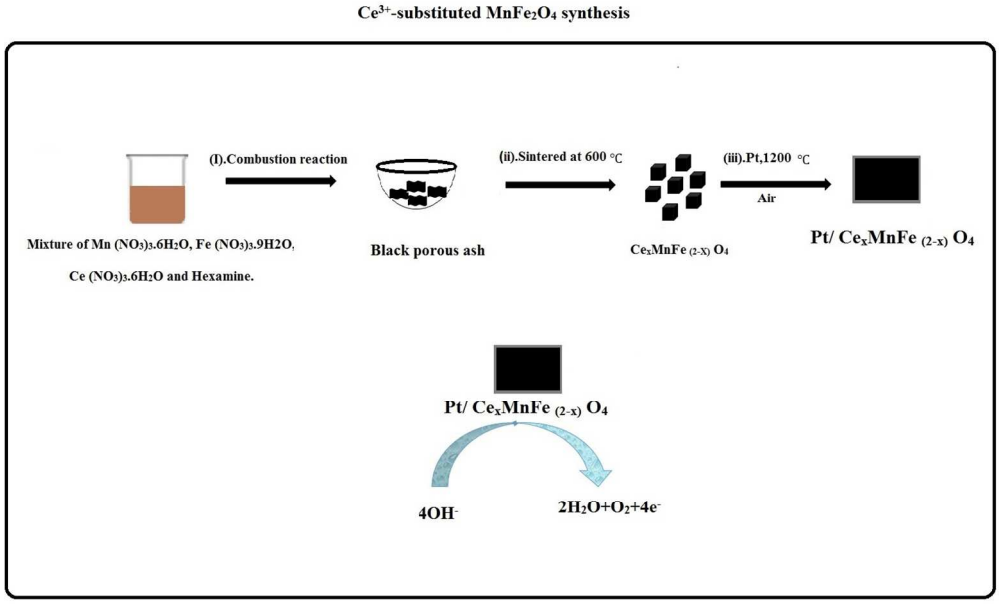

404x245mm (96 x 96 DPI)

Enhancing the electro catalytic activity of manganese ferrite through cerium substitution for oxygen evolution in KOH solutions

T.Pandiarajan and S.Ravichandran*

CSIR - Central Electrochemical Research Institute, Karaikudi-630006, India.

* Corresponding Author.

E-mail:Srravi371@gmail.com.

Abstract:

Alkaline water electrolysis (AWE) is the simplest way of producing hydrogen, an attractive fuel for the future. In view of cost-effectiveness and durability, non-noble metal oxides are the promising catalysts for AWE. Here, we studied the effect of Ce substitution on the OER activity of manganese ferrite. Ce substituted $MnFe_2O_4$ ($0 \leq x \leq 0.8$) was synthesized by a combustion method. Characterization techniques such as SEM, XRD, EDAX and XPS were used to analyse the surface morphology and the chemical composition of $Ce_xMnFe_{(2-x)}O_4$. Substitution of Ce^{3+} in the cubic lattice of $MnFe_2O_4$ increases the conductivity of $Ce_xMnFe_{(2-x)}O_4$, which results in the negative shift in the OER onset potential. Among all Ce^{3+} substituted manganese ferrites, $Ce_{0.2}MnFe_{1.8}O_4$ was found to be more active for OER in terms of current and stability. Notably, $Ce_{0.2}MnFe_{1.8}O_4$ affords a current density of 10 mA/cm^2 at a small overpotential of ~0.310m V and a Tafel slope value of 31 mV/decade, these values are comparable to the well-investigated non-noble metal oxides.

Key words: Alkaline water electrolysis, Non-noble metal oxides, Ce-substituted $MnFe_2O_4$, OER, Cubic lattice.

1. Introduction

Our world has moved steadily towards a serious energy crisis, which has sparked dedicated research related to renewable energy, storage, and conversion technologies. In pursuit of the ultimate energy source, developing solar water-splitting cell, batteries, and fuel cells are of current research focus. As a result of the sluggish kinetics involved in the oxygen evolution reaction (OER) and hydrogen evolution reaction (HER) sustainable energy systems require a large input of energy[1,2,3]. Metal oxides composed of iridium and ruthenium exhibit excellent catalytic activity for the oxidation of water into molecular hydrogen and oxygen; however, high cost and scarcity make these oxides undesirable for commercial applications[4]

Although electrolytic water splitting was first identified in an acidic medium, because of cost-effective electrolyser fabrication and the simple control of corrosion, alkaline water electrolysis has dominated large-scale hydrogen production technology for several decades. Still, it has been challenge to find non-noble metal catalysts that exhibit a current density of j > 0.5 A cm^{-2} at an over potential of η_{O2}<0.3V with long-term stability.[5,6,]

The exhaustive search for non–noble catalysts has identified that the mixed metal oxides of transition elements, spinel ferrites, oxy hydroxides (such as MnO_2, NiO_X, $MnFe_2O_4$, $NiFe_2O_4$, $CoFe_2O_4$, Co_3O_4,etc.) and perovskites oxides, as catalysts for OER reaction[2,6–10] . Importantly, Inspired by the oxygen evolution centres (OEC) of photosystem II, several investigations of low-cost manganese oxides for electrochemical water splitting revealed the efficiency of MnO_2 and Mn_3O_4 for OER, particularly the α-Mn2O3 phase. While MnO_2 is a potential bifunctional catalyst in both acidic and basic mediums, changing the pH from alkaline to neutral results in a sharp increase in the onset potential [11–14].

Surprisingly, spinel ferrites and mixed metal oxides NPs supported with graphene or carbon nanotube potentially support the ORR in alkaline solutions[2,9].However, their performance also drops significantly on conventional carbon supports. But, Spinel ferrites($MxFe_{3-x}O_4$) NPs supported with conventional carbon exhibit better ORR activity compared to commercial Pt NPs in alkaline solution[15].

However, the spinel ferrites possessing significant electro catalytic activity and stability in high pH, the low electrical conductivity, restricts its application as a catalyst. In general, the practical applications of ferrites are mainly depends on electronic conductivity, results from thermal activation of electrons or positive holes along chains of neighbouring cations in the ionic lattice. Due to the bimetallic nature of spinels, the conductivity of ferrites can be tuned by substituting with a foreign metal, using different preparation conditions or using heat treatment[16–18].

Previous studies of $MnFe_2O_4$ employed several synthesis methods, mostly to examine structural, electrical conductivity, Magnetization and OER properties [19,20]. Recently, Shouheng Sun and his co-works found that similar ferrite system exhibits the ORR activity in alkaline solution, comparable to that of Pt[15].The focus of our current study involves determining the catalytic behaviour of cerium substituted manganese ferrite, for OER in alkaline solution. We prepared manganese ferrite and cerium-substituted manganese ferrites by a combustion method [18].Electro catalytic analysis showed that $Ce_{0.2}MnFe_{1.8}O_4$ is a promising catalyst for OER in alkaline solutions.

2. Experimental section

2.1. Synthesis of catalysts:

Manganese ferrite and cerium substituted manganese ferrites were synthesized by a combustion method. Aliquot amounts of analytical grade metal nitrates, Mn $(NO_3)_2.6H_2O$, Fe $(NO_3)_2.9H_2O$ and Ce $(NO_3)_3.6H_2O$ were mixed with hexamine and dissolved in deionized water to obtain a precursor solution. The solution was preconcentrated in a quartz crucible until the free water evaporated, after which spontaneous combustion of the dried powder occurred. This resulted in the formation of black porous ash in the container. This ash was then sintered at 1100ºC for 24 hours in an electrical furnace. The catalyst was milled for 8 hours in a Retsch PM 100 ball mill at room temperature at 600 rpm. For milling experiments, the ball-to-powder weight ratio was taken as 40:1.

2.2. Physiochemical characterization:

Catalyst crystallinity and structure examined by a powder X-ray diffractometer (Model D8 Advance, Bucker) with a Cu- Kα1 X-ray radiation (λ = 0.15406 nm) source, operating at 40 kV and 30 mA. Catalyst morphology and surface composition investigated using a VEGA3 TESCAN Scanning Electron Microscope, with Energy Dispersive X-ray Spectroscopy (SEM/EDS) with X-Flash Detector 410M with Bruker ESPRIT QUANTAX EDS analysing software. X-ray photoelectron spectroscopy (XPS) was carried out on MULTILAB 2000 Base system with X-Ray, Auger and ISS attachments (Thermo scientific) with Twin Anode Mg/Al (300/400W) X-Ray Source.

2.3. Working electrode preparation

The suspension of catalyst was prepared by sonicating 3mg of the catalyst, in 60 μL isopropyl alcohol for 15minutes.30 μL of the suspension was pipetted out and dried on a metal substrate (1cm×1cm) by heating, in a pre-heated oven at 80°C. Subsequently the substrate was sintered, at 1200°C in the presence of air for 2 hours.

2.4. Electrochemical measurements:

Electrochemical experiments were conducted at room temperature using a VMP3 multi-channel potentiostat produced by the Bio-Logic Science Instrument Company. In the three-electrode system, a Pt wire was used as counter electrode, and all potentials were measured with respect to 1 M KOH Hg/HgO reference electrode that was housed in a custom glass Luggin capillary. The potential of the 1 M KOH Hg/HgO reference electrode was 0.929 V. All potentials during electrochemical characterization were IR-compensated and reported versus RHE. The scan rate was 1 mVS^{-1} for all electrochemical measurements except during the cyclic voltammetry studies. All cyclic voltammograms were measured in a 1 M KOH electrolyte with a sweep rate of 10 mV/s. Three KOH solutions, 0.01M, 0.1M, and 1.0M, were used as electrolytes. Electrochemical impedance spectroscopy (EIS) measurements were conducted in the frequency range 1 MHz to 10 Hz, 1.6V versus RHE, with an AC voltage amplitude of 10 mV.

The x-ray diffraction patterns of the as prepared $MnFe_2O_4$ with different concentrations of Ce^{3+} ions from 0.0M to 0.8M are as shown in Fig.3a. The reflection patters are distinct, clearly delineating the cubic phase of the spinels. Moreover, no typical diffraction peak for MnO_2 (110) or Ce_2O_3 (111), (220) is seen in the XRD pattern for MnFe2O4, which reveals that the samples are not composites. The sharp, well-defined peaks display the crystalline

nature of the spinel ferrites. As shown in fig.3a no changes occurred in the position of the reflections due to the inclusion of Ce^{3+} for Fe^{3+} , only a variation in the lattice constant values were observed because of a great deviation in the ionic radius of metal ions (Ce^{3+}=1. 3Å; Fe^{3+}=0. 64 Å). The variation of lattice constant values derived from XRD data are given in fig (3b). A similar behaviour of lattice parameter with La^{3+} substitution is observed by *L. J. Berchmans et.al* in a similar ferrite system.[17, 21]

Fig. (2). shows the chemical composition of pt/$MnFe_2O_4$ electrodes (sintering at 1200℃, in the presence of air for 2 hours) estimated by energy-dispersive X-ray (EDX) analysis, which revealed that the catalysts contained only Mn, Fe and O atoms in a ratio of 1:2:4. The absence of Pt in the EDX profile shows that no diffusion of platinum occurs during the high temperature treatment (Fig.5).Moreover, the EDS measurements confirm the presence of Ce in the $MnFe_2O_4$ lattice in the calculated ratio (Figure. 2). The XPS spectrum, shown in Figure (4), was also used to verify the presence of Ce^{3+}. The characterized peaks at 845 eV and 905 eV in the XPS spectra occurs due to the presence of Ce^{3+}.[22] Based on the above results, we conclude that Ce^{3+} is present in our samples.

The morphology of the as-prepared $MnFe_2O_4$ and substituted $MnFe_2O_4$ are confirmed by the SEM images Fig [1a]. All the particles have discrete crystals with a cube shape. Each sample is then dispersed in isopropyl alcohol (IPA) and coated on Pt (1cm x 1cm) electrode. As shown in fig.1b, sintering the electrode to 1200ºC leads to the melting of discrete $MnFe_2O_4$ particles, resulting in the agglomeration of ferrite particles together to form a single, thin, film-like layer on the Pt surface.[10] The sintering process favours the formation of a thin flim of spinel ferrites on Pt surface; however, no characterise peak for pt is observable in XRD analysis, which accounts for absence of Pt diffusion into the spinel ferrites. Thin flim layer

insulates the pt surface completely. Also, no redox peak appeared for Pt on cyclic voltammetry studies of samples in KOH solution.

Fig. [5] shows the corresponding cyclic voltammograms of pt/$Ce_XMnFe_{2-X}O_4$ with x =0.0,0.2,0.4,0.6,0.8 at a potential scan rate of 10 mV s^{-1} in 1M KOH solution at 25 ℃.The electrode surface of the Pt/$Ce_XMnFe_{2-X}O_4$ did not show any redox peaks either for Pt or for catalyst on cyclic voltammetry studies.[19] It implies that ferrite does not undergo further oxidation. R.N.Singh and co-workers reported the similar behaviour for Mn-substituted ferrites coated on Pt and Ti substrates (Reference.19).

However, with each subsequent CV cycle, OER current increases and OER onset potential shifted towards more negative region due to incorporation of $Ce3^+$. It is often considered that the effect of Ce^{3+} incorporation on $MnFe_2O_4$ enhances the electrical conductivity of materials in turn influencing the OER activity.

The polarisation curves of pt/$Ce_xMnFe_{2-x}O_4$ electrodes were performed in1M KOH solution fig. (7). The Pt /$MnFe_2O_4$ electrode prepared by current method shows an over potential of 360 mV for OER which is lower than the reported value of 580mV for $MnFe_2O_4$ electrodes by **Iwakura *et al*** [23]. Related to pure $MnFe_2O_4$ a negative shift in the OER onset potential is noticed with all Ce substituted electrodes. Among all, the $Ce_{0.2}MnFe_{1.8}O_4$ exhibits a maximum negative shift of 60mV for OER lower than $MnFe_2O_4$. Comparison of over potentials of the various catalysts required to achieve a current density of 10mA/cm^2 for CexMnFe $_{(2-x)}$ O_4 are shown in fig. [7]. In a similar condition, **Iwakura et al.** [23] observed an over potential of 440mV and 580mV for $CoFe_2O_4$ and $MnFe_2O_4$ in 1M KOH respectively. Similarly, Orehotsky et al. obtained the same current density at the over potential of 340mV

for NiFe2O4 in 30wt% KOH [19]. In addition, our results are comparable to well investigated Cobalt-based electrocatalysts.

A negative shift in the OER onset is associated with incorporation Ce^{3+} in the $MnFe_2O_4$ spinel lattice. As shown in fig.6 the electrochemical impedance plots of $Ce_xMnFe_{2-x}O_4$ exhibit low charge transfer resistance compared to pure $MnFe_2O_4$ electrodes. Because of the reduced charge transfer resistance the electronic conductivity increases and favours in the enhancement of electro catalytic activity Ce^{3+} substituted $MnFe_2O_4$. Typically, manganese ferrite has inverse spinel structure in which 80% of Mn^{2+} occupies site A and 20% occupies site B. Site B can also be occupied by Fe^{2+} and Fe^{3+} ions.[24,25] The electrical conductivity of ferrites are explained by Verwey-de Boer mechanism and the polaron effect. Although the electrical conduction in ferrites originates between Fe^{2+} and Fe^{3+} ions at site B, conduction mainly depends on the Fe^{2+} concentrations. In the sintering process, some lattice oxygen escapes from the oxides, causing an oxygen deficiency in the crystal lattice. Therefore, to balance the electrical charge created in the lattice unit, $Fe^{3+}$is reduced to Fe^{2+}.[24,26] The X-ray photoelectron spectroscopy (XPS) spectrum, shown in figure (4), confirms the existence of Fe^{2+} ions in the spinel lattice, and the presence of two main peaks with binding energies of 710.4 and 724.8 eV, which clearly proves that Fe^{2+} coexists with Fe^{3+}.[27,28] Moreover, it was found that the created Fe^{2+} ions prefer to occupy the octahedral B-sites. This reduction facilitates the formation of excess Fe^{2+} ions in the system (as shown in figure .4(b)) such that the hopping rate of electrons in ferrites increases which is the cause of their higher electronic conductivity.[24,29] If it is the only cause then, we could expect a gradual increase in catalytic activity of substituted $MnFe_2O_4$ with higher concentrations of Ce^{3+}.In contrast, the OER onset potential increased at concentrations higher than 0.2M. Because, the replacement of rare earth ions forms grain boundaries in ferrites[30] ; if high molar concentration is used, then it leads to the formation of secondary phases(i.e. ABO_3) on the materials[16,17]. Most importantly, the

secondary phase exists at concentration >0.4. Although the density of these grain boundaries is reduced upon treating the powders at high temperature, secondary phase are still present in the catalyst layer at high concentrations of cerium; which may hinder the mobility of charge carriers and increases the electrical resistivity.[31] Similar behaviour was found in Al doped Manganese ferrites[19]. This coincides with the negative shift of OER onset potential.

As a result, of the cooperative effect[32] between the electron-rich Mn^{2+} and Ce^{3+}centres in the cubic spinel lattice also enhances the OER activity of $Ce_{0.2}MnFe_{1.8}O_4$ [17]. Nevertheless, both effects work simultaneously and increase the electro catalytic activity of the substituted manganese ferrite. It is clear from the above discussion that the electronic and structural properties of spinels play an important role in the OER.

The iR corrected Tafel slope values of the $Ce_xMnFe_{(2-x)}O_4$ are calculated from the steady state polarization plots shown in fig. [8] using the following equation:

$$\eta = a + b\ log\ j \rightarrow \qquad (1)$$

We also obtained a range of Tafel slope values varying from 31-45mV/decade for all oxides, which is similar to the previous reports[19,23].

The reaction order (p) of $Ce_{0.2}mnfe_{1.8}O_4$ and pure $MnFe_2O_4$ with respect to [OH^-] are calculated by the method described in ref. [18]. The calculated P and b values are in good agreement with recently reported spinel ferrites such as $MnFe_2O_4$ (b=36mV/decade, p=1.9), $Cr_xMnFe_{2-x}O_4$ (b=35mV/decade, p=2) and $Cr_xCoFe_{2-x}O_4$ *(b*1 =40–51*, b*2 =60–89mV/decade, *p* = 1.2–1.4*)*. Besides, similar electrode kinetic parameters also exhibited by $NiCo_2O_4$ film *(b* = 42mV/decade*, p* = 1.7*)* and$CuCo_2O_4$ (b=40mV/decade) sprayed on Ni[19,23].

Based on the Tafel slope value and oxygen evolution potential, the sequential order of the electro catalytic activity of the electrodes is given as $Ce_{0.2}MnFe_{1.8}O_4$>$Ce_{0.4}MnFe_{1.6}O_4$> $Ce_{0.6}MnFe_{1.4}O_4$> $Ce_{0.8}MnFe_{1.2}O_4$ >$MnFe_2O_4$.

In addition, the Tafel slope measurements attribute to the common mechanism for OER reaction as well:

$$S + OH^- \leftrightarrow SOH + e^- \quad (2)$$

$$SOH + OH^- \leftrightarrow SO^- + H_2O \quad (3)$$

$$SO^- \leftrightarrow SO + e^- \quad (4)$$

$$2SO \leftrightarrow 2S + O_2 \quad (5)$$

Where, **S** indicates the active species on the catalyst surface.

R.N.Singh and co-workers [19] observed a tafel slope (b) value of 36-47mV/decade in 1M KOH at 25℃, suggesting that $Mn_xFe_{2-x}O_4$ follows second order kinetics with respect to [OH^-] and step (3) as the rate determining step(RDS) for OER. We also observed a similar trend in tafel slope values and reaction rate in case of $MnFe_2O_4$ (b=38mV/decade; p=2.0) and $Ce_{0.2}MnFe_{1.8}O_4$ (b=31mV/decade; p=1.9). The long-term stability of $Ce_{0.2}MnFe_{1.8}O_4$ under OER conditions was determined using chronoamperometric studies. The electrode is kept at a constant potential of 1.8V for 10 h in 1M KOH solution, while the current was measured as a function of time. Stability of the electrode found to be unchanged throughout the constant-potential studies with a constant current density of 130mA/cm^2 (Figure. 9).

Conclusion:

Ce -substituted $MnFe_2O_4$ powders with varying concentration of Ce were prepared by the combustion method .The X-ray diffraction patterns of the samples confirm the cubic structure of the spinels. Substitution of Ce^{3+} for Fe^{3+} decreases the OER onset potential for about 50mV, which may be explained by the electronic conductivity and cooperative effect. Among all samples, $Ce_{0.2}MnFe_{1.8}O_4$ showed the maximum electronic conductivity and OER activity. The chronoamperometric study of Ce0.2MnFe1.8O4 reveals the long-term stability of the catalyst.

Acknowledgements:

The authors thank UGC, India for providing junior research fellowships.

REFERENCES:

1. M. W. Kanan and D. G. Nocera, Science, 2008, **321**, 1072-1075.
2. Y. Liang, Y. Li, H. Wang, J. Zhou, J. Wang, T. Regier and H. Dai, Nature materials, 2011, **10**, 780-786.
3. C. C. McCrory, S. Jung, J. C. Peters and T. F. Jaramillo, J Am Chem Soc, 2013, **135**, 16977-16987.
4. T. Reier, M. Oezaslan and P. Strasser, ACS Catalysis, 2012, **2**, 1765-1772.
5. . E. Rasten, G. Hagen and R. Tunold, Electrochimica Acta, 2003, **48**, 3945-3952.
6. Y. Leng, G. Chen, A. J. Mendoza, T. B. Tighe, M. A. Hickner and C. Y. Wang, Journal of the American Chemical Society, 2012, **134**, 9054-9057.
7. W. Zhou and J. Sunarso, The Journal of Physical Chemistry Letters, 2013, **4**, 2982-2988.
8. . R. D. Smith, M. S. Prevot, R. D. Fagan, Z. Zhang, P. A. Sedach, M. K. Siu, S. Trudel and C. P. Berlinguette, Science, 2013, **340**, 60-63.
9. Y.Gorlin and T. F. Jaramillo, Journal of the American Chemical Society, 2010, 132, 13612-13614.
10. S.Ida, K.Yamada, T.Matsunaga, H.Hagiwara, Y, Y, Y. Matsumoto and T. Ishihara, Journal of the American Chemical Society, 2010, 132, 17343-17345.

11. T. Takashima, K. Hashimoto and R. Nakamura, Journal of the American Chemical Society, 2012, **134**, 1519-1527.

12. T. Takashima, K. Hashimoto and R. Nakamura, Journal of the American Chemical Society, 2012, **134**, 18153-18156.

13. D. M. Robinson, Y. B. Go, M. Mui, G. Gardner, Z. Zhang, D. Mastrogiovanni, E. Garfunkel, J. Li, M. Greenblatt and G. C. Dismukes, Journal of the American Chemical Society, 2013, **135**, 3494-3501.

14. D.M. Robinson, Y.B.Go, M.Greenblatt, and G.C.Dismukes, Journal of the American Chemical Society, 2010, **132**, 11467-11469.

15. H. Zhu, S. Zhang, Y. X. Huang, L. Wu and S. Sun, Nano letters, 2013, **13**, 2947-2951.

16. J. Z. Msomi, T. Moyo and J. J. Dolo, Hyperfine Interact, 2010, **197**, 59-64.

17. R. Singh, J. Singh, H. Nguyencong and P. Chartier, International Journal of Hydrogen Energy, 2006, **31**, 1372-1378.

18. L. J. Berchmans, M. P. I. Devi and K. Amalajyothi, International Journal of Self-Propagating High-Temperature Synthesis, 2009, **18**, 11-14.

19. N. K. Singh, S. K. Tiwari, K. L. Anitha and R. N. Singh, Journal of the Chemical Society, Faraday Transactions, 1996, **92**, 2397.

20. K. Mujasam Batoo, Physica B: Condensed Matter, 2011, **406**, 382-387

21. J. Xiang, X. Shen and Y. Zhu, Rare Metals, 2009, **28,** 151-155.

22. **J.** Hou, W. Jiang, Y. Fang and F. Huang, Journal of Materials Chemistry C, 2013**, 1,** 5892.

23. C. Iwakura, M. Nishioka and H. Tamura, Nippon Kagaku Kaishi, 1982, **7,** 136.

24. Y. Fukuda, S. Nagata and K. Echizenya, Journal of Magnetism and Magnetic Materials, 2004, **279**, 325-330.

25. B. Liu, K. Zhou, Z. Li, D. Zhang and L. Zhang, Materials Research Bulletin, 2010, **45**, 1668-1671.

26. A. Tawfiks, Y. Atassi, and I.S. Daewish, 2005, 68-74.

27. Y. Fu, P. Xiong, H. Chen, X. Sun and X. Wang, Industrial & Engineering Chemistry Research, 2012, **51**, 725-731.

28. L. Zhang and Y. Wu, Journal of Nanomaterials, 2013, 2013, 1-6.

29. B. Parvatheeswara Rao and K. H. RAO Journal of Materials Science, 1997, **32**, 6049 – 6054.

30. X.jun, S.Xiangqian, and Z.Yongwei, Rare Metals, 2009, **28**,151.

31. A. A. Sattar, and A.M.Samy, Journal of Material Science, 2002, **37** 4499 – 4502.

32. D.W.stephan, Coord Chem Rev, 1989, **95, 41**.

FIGURE CAPTIONS

Figure 1. SEM images of as prepared $Ce_xMnFe_{2-x}O_4$ samples.

Figure 1a.SEM images of sintered samples at 1200 ^{0}C.

Figure 2. EDAX spectrum of catalysts after sintering at 1200 ^{0}C.

.

Figure 3a. XRD patterns of (i) $MnFe_2O_4$ (ii) $Ce_{0.2}MnFe_{1.8}O_4$ (iii) $Ce_{0.4}MnFe_{1.6}O_4$ (iv). $Ce_{0.6}MnFe_{1.4}O_4$ (v) $Ce_{0.8}MnFe_{1.2}O_4$.

Figure 3b.The Variation of Lattice constant (a) with **X** of $Ce_XMnFe2_{-X}O_4$.

Figure 4.XPS spectra of the catalysts. The insert (a) is survey spectra of as prepared $Ce_{0.2}MnFe_{1.8}O_4$, (b) XPS spectra of Fe before sintering (c) XPS spectra of Ce before sintering (d) XPS spectra of Fe (after sintered at 1200℃).

Figure 5. Cyclic voltammograms of Pt supported $MnFe_2O_4$ and $Ce_xMnFe_{2-x}O_4$ electrodes at a potential scan of 10mV/s in 1M KOH at 25℃.

Figure 6. Electrochemical impedance spectra of catalysts as a function of Ce substitution, measured at 1.6V during oxygen evolution.

Figure 7.Polarisation curves of $Ce_xMnFe_{2-x}O_4$ sintered on Pt (with catalyst loading of 1 mg cm^2) measured in 1MKOH.

Figure 8. Tafel plots of $MnFe_2O_4$ and $Ce_xMnFe_{2-x}O4$ coated on Pt recorded at 1 mV/s in 1 M KOH.

Figure 9. Chronoamperometric curves of $MnFe_2O_4$ and $Ce_{0.2}MnFe_{1.8}O4$ loaded on Pt under potential of 1.8V.

TABLE CAPTIONS

Table.1 Tafel slope values of $Ce_xMnFe_{2-x}O_4$.

Table.2.Catalytic activity of various electrodes in 1MKOH.

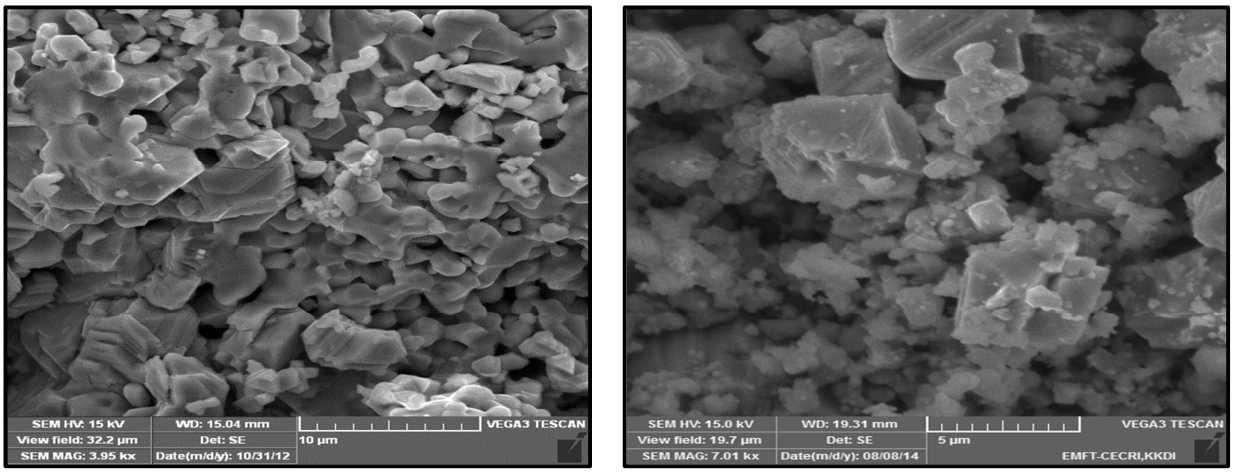

Figure: 1

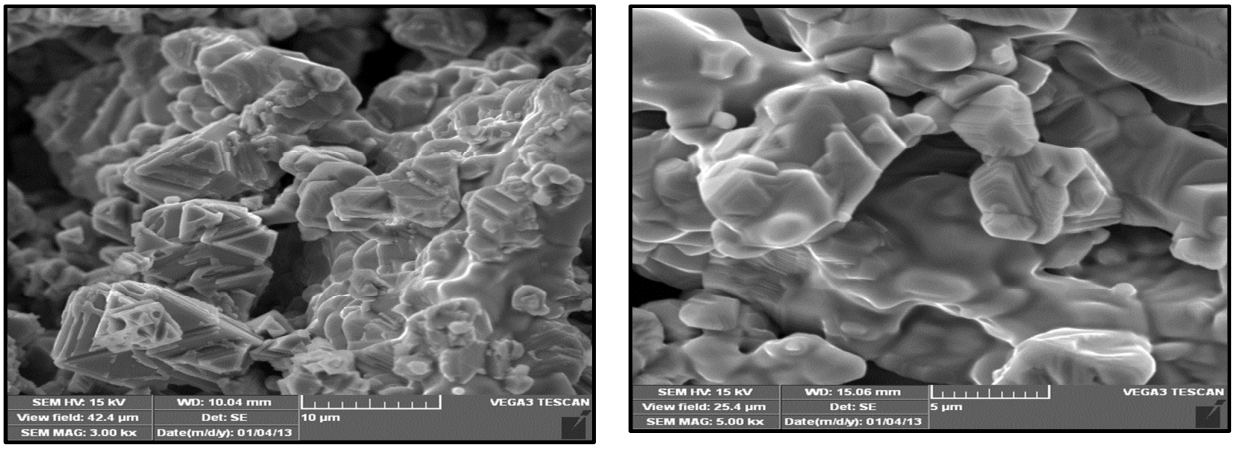

Figure: 1a

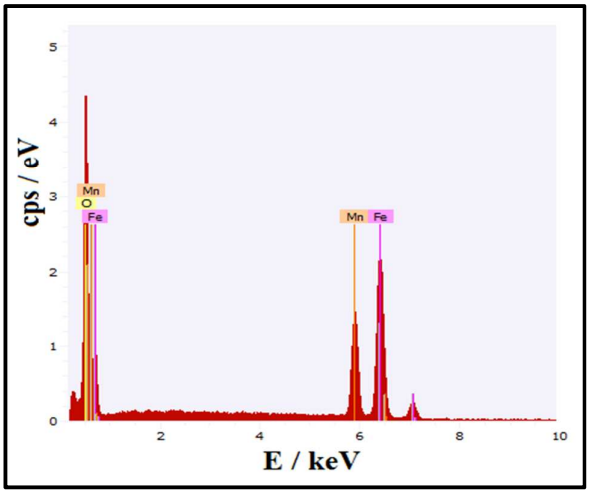

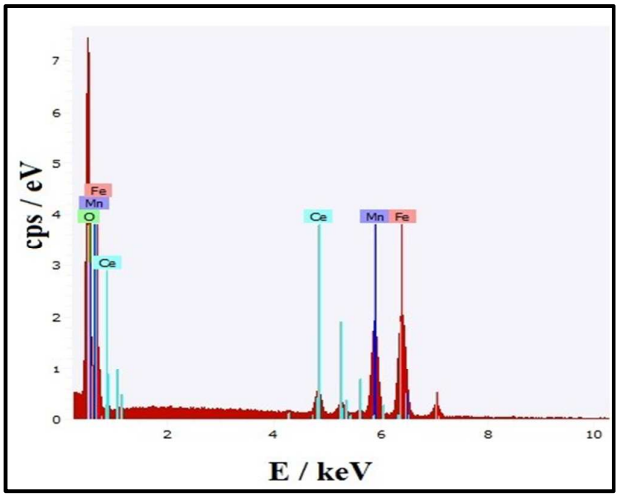

Figure: 2

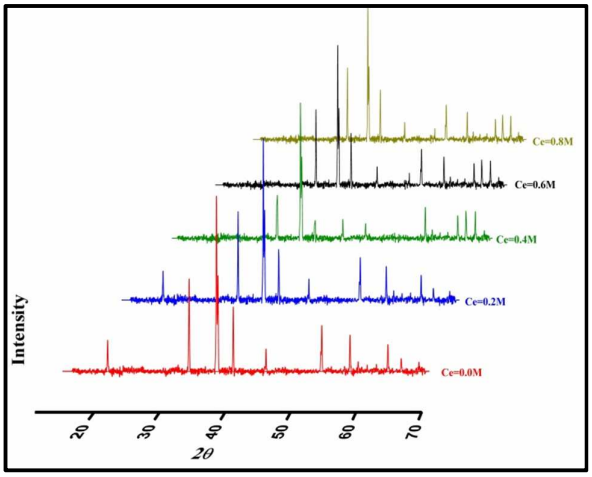

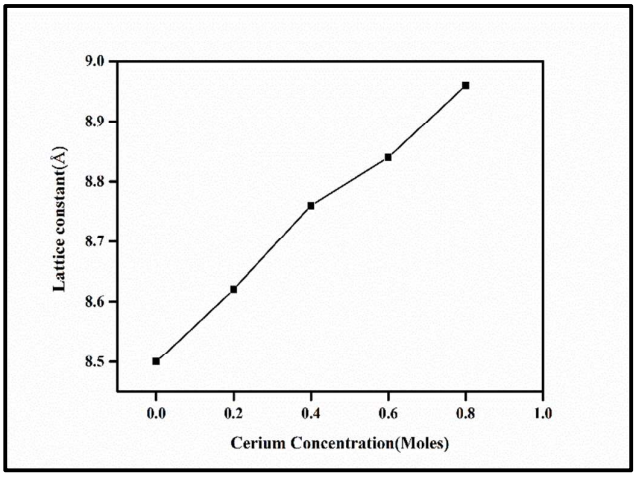

Figure: 3a

Figure: 3a

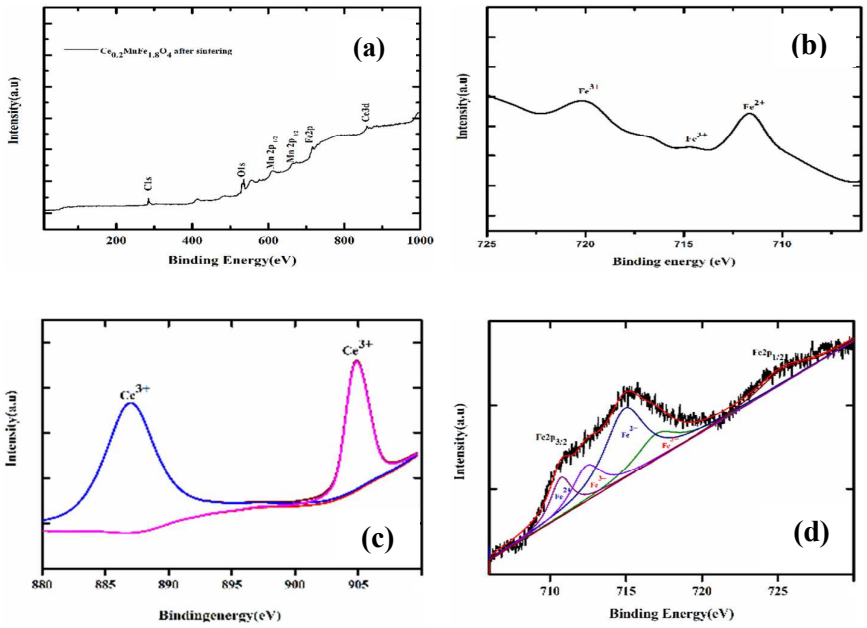

Figure: 4

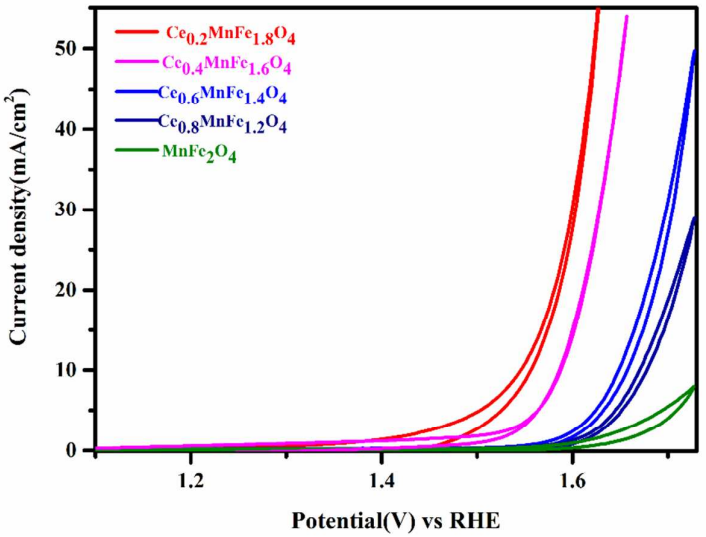

Figure: 5

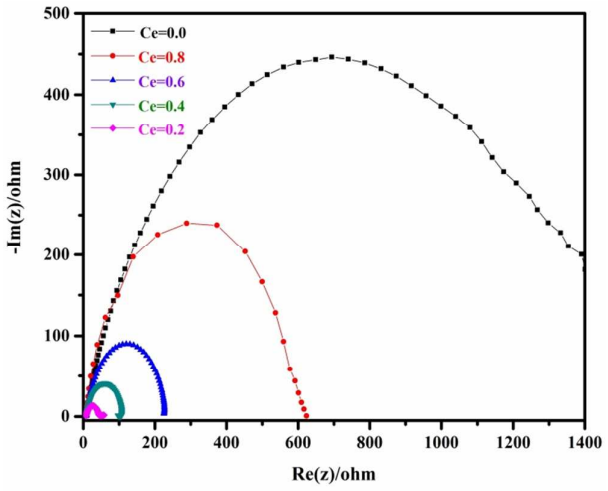

Figure: 6

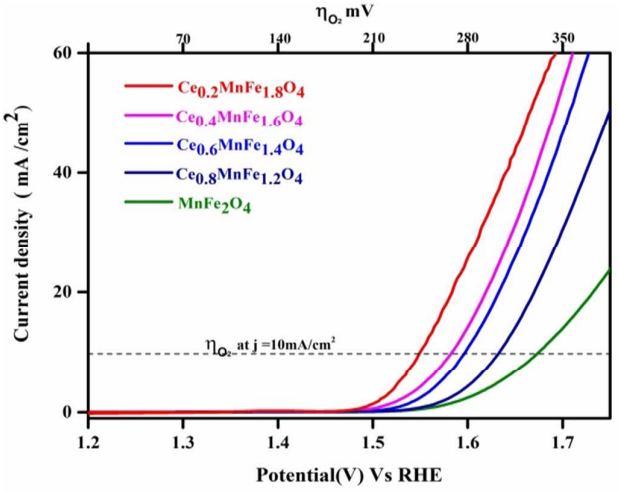

Figure: 7

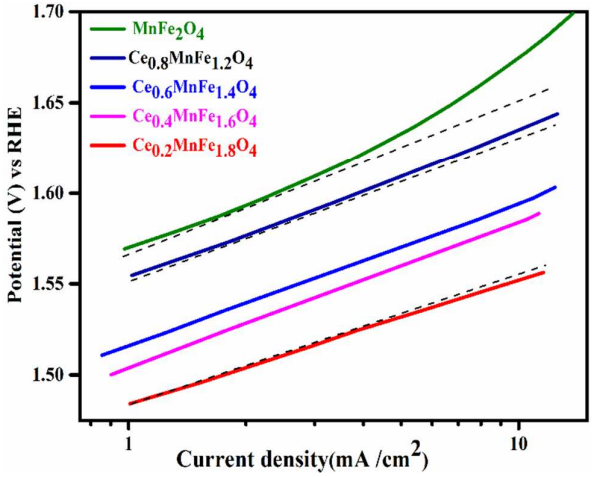

Figure: 8

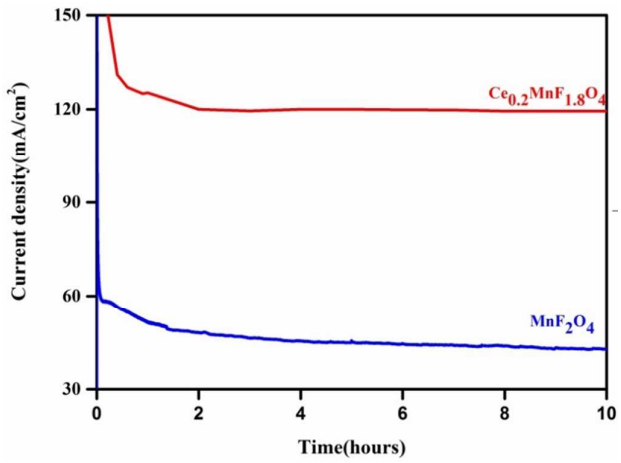

Figure: 9

Tables:

S.No	catalyst	Tafel slope (b)mV/decade
1.	$MnFe_2O_4$	**38**
2.	$Ce_{0.2}MnFe_{1.8}O_4$	**31**
3.	$Ce_{0.4}MnFe_{1.6}O_4$	**33**
4.	$Ce_{0.6}MnFe_{1.4}O_4$	**35**
5.	$Ce_{0.8}MnFe_{1.2}O_4$	**37**

Table: 1

S.No	Electrodes	KOH Concentration & Temperature	OER potential (mV) at $10mA/cm^2$	Tafel slope value(b) mV/decade	Reference
1	$Pt/Ce_{0.2}MnFe_{1.8}O_4$	1M ,25℃	310	31	this work
2	$Ni/MnFe_2O_4$	1M ,25℃	300	36-42	ref.19
3	$Pt/MnFe_2O_4$	1M ,25℃	580	110-115	ref.23
4	$Pt/ CoFe_2O_4$	1M ,25℃	440	110-115	ref.23
5	$NiFe_20_4$	30wt.%,25℃	340	-	ref.19
6	Ni/Co_3O_4/N-rmGO	1M,25℃	310	67	ref.02
7	$NiLaO_x$	1M,25℃	400	-	ref.03

Table: 2